

Charged and metallic molecular monolayers through surface-induced aromatic stabilization

G. Heimel^{1*}, S. Duhm^{2*}, I. Salzmann¹, A. Gerlach³, A. Strozecka⁴, J. Niederhausen¹, C. Bürker³, T. Hosokai^{3,5}, I. Fernandez-Torrente⁴, G. Schulze⁴, S. Winkler^{1,6}, A. Wilke¹, R. Schlesinger¹, J. Frisch¹, B. Bröker¹, A. Vollmer⁶, B. Detlefs⁷, J. Pflaum⁸, S. Kera⁹, K. J. Franke⁴, N. Ueno⁹, J. I. Pascual^{4†}, F. Schreiber³ and N. Koch^{1,6}

Large π -conjugated molecules, when in contact with a metal surface, usually retain a finite electronic gap and, in this sense, stay semiconducting. In some cases, however, the metallic character of the underlying substrate is seen to extend onto the first molecular layer. Here, we develop a chemical rationale for this intriguing phenomenon. In many reported instances, we find that the conjugation length of the organic semiconductors increases significantly through the bonding of specific substituents to the metal surface and through the concomitant rehybridization of the entire backbone structure. The molecules at the interface are thus converted into different chemical species with a strongly reduced electronic gap. This mechanism of surface-induced aromatic stabilization helps molecules to overcome competing phenomena that tend to keep the metal Fermi level between their frontier orbitals. Our findings aid in the design of stable precursors for metallic molecular monolayers, and thus enable new routes for the chemical engineering of metal surfaces.

Electronically, the fundamental difference between molecules, organic semiconductors in particular, and metals is that the former exhibit a finite gap between their highest occupied and lowest unoccupied molecular orbitals (HOMO and LUMO, respectively), whereas the latter are characterized by a continuous density of states (DOS) around their Fermi energy E_F (Fig. 1a). An obvious question is what happens when two such dissimilar materials are brought into contact. Indeed, understanding the structure and electronic properties of interfaces between metals and π -conjugated molecules has been the focus of intense research for decades^{1–3}, not only because of a fundamental scientific interest, but also because of the technological relevance of such interfaces in, for example, organic and molecular electronic devices^{4–6}.

One of the central issues is whether an organic semiconductor on a metal surface retains its intrinsic electronic characteristics: does it remain semiconducting with its HOMO entirely below the Fermi level, its LUMO above and the continuum of delocalized electronic states at E_F residing predominantly on the metal (Fig. 1b)? Or is it, in contrast, possible to obtain a continuum of hybrid metal–organic states at E_F that exhibit pronounced frontier-orbital (for example, LUMO) character on the molecular side (Fig. 1e)? As these states seamlessly extend over both material components, the organic adlayer can be regarded as having ‘inherited’ the metallic character of the substrate in the latter case. This not only raises deep-rooted questions on the meaning of conceptually separating molecule and metal in such a scenario, but it also harbours the technological potential of realizing ‘soft’ molecular contacts to organic and

biological matter⁷, which, nevertheless, behave metallically for all practical purposes.

The archetypical pentacene (PEN), like the majority of organic semiconductors, stays semiconducting on the (111) surfaces of coinage metals^{8–11}. Even lowering its frontier orbitals by ~ 1.0 eV through full fluorination (Fig. 1d)^{12,13} does not lead to occupied LUMO-derived states in the resulting perfluoropentacene (PFP)^{10,11,14}. In contrast, several acceptor molecules, which generally exhibit strongly electron-withdrawing groups on the periphery of a π -conjugated core, do exhibit a substantial LUMO-related DOS at (or even entirely below) the Fermi level of some metal surfaces^{7,15–27}. Although each of these has been investigated separately in some detail, to date no overarching concept exists that explains why some molecules more readily permit their LUMO to be (partially or entirely) filled than do others.

Naively, one could assume it to be only a matter of the acceptor strength of the organic adsorbate, that is, its LUMO energy. In the present study, we employ a comprehensive set of complementary experimental techniques, supported by state-of-the-art electronic structure calculations, to demonstrate that this is not the case. For reasons that will successively become clear below, we focus on 6,13-pentacenequinone (P2O) and 5,7,12,14-pentacenetetrone (P4O) to elucidate an additional mechanism that we find plays a central role in the occurrence of partially occupied frontier molecular orbitals on metal surfaces. Their chemical structures (Fig. 1f,g) reveal that these generic names are somewhat misleading: In contrast to PEN, which exhibits a fully π -conjugated backbone, P2O should be better regarded as two naphthalene units linked together

¹Institut für Physik, Humboldt-Universität zu Berlin, Brook-Taylor-Straße 6, D-12489 Berlin, Germany, ²Jiangsu Key Laboratory for Carbon-Based Functional Materials & Devices, Institute of Functional Nano & Soft Materials (FUNSOM), Soochow University, Suzhou 215123, China, ³Institut für Angewandte Physik, Universität Tübingen, Auf der Morgenstelle 10, D-72076, Tübingen, Germany, ⁴Fachbereich Physik, Freie Universität Berlin, Arnimallee 14, 14195 Berlin, Germany, ⁵Department of Materials Science and Technology, Iwate University, 4-3-5 Ueda, Morioka, Iwate 0208551, Japan, ⁶Helmholtz Zentrum Berlin für Materialien und Energie GmbH, D-12489 Berlin, Germany, ⁷European Synchrotron Radiation Facility, 6 Rue Jules Horowitz, BP 220, 38043 Grenoble Cedex 9, France, ⁸Experimental Physics VI, University of Würzburg and ZAE nanoGUNE, 97074 Würzburg, Germany, ⁹Graduate School of Advanced Integration Science, Chiba University, Chiba 263-8522, Japan; [†]Present address: CIC nanoGUNE, 20018 Donostia-San Sebastian, and Ikerbasque, Basque Foundation for Science, 48011 Bilbao, Spain. *e-mail: georg.heimel@physik.hu-berlin.de; duhm@suda.edu.cn

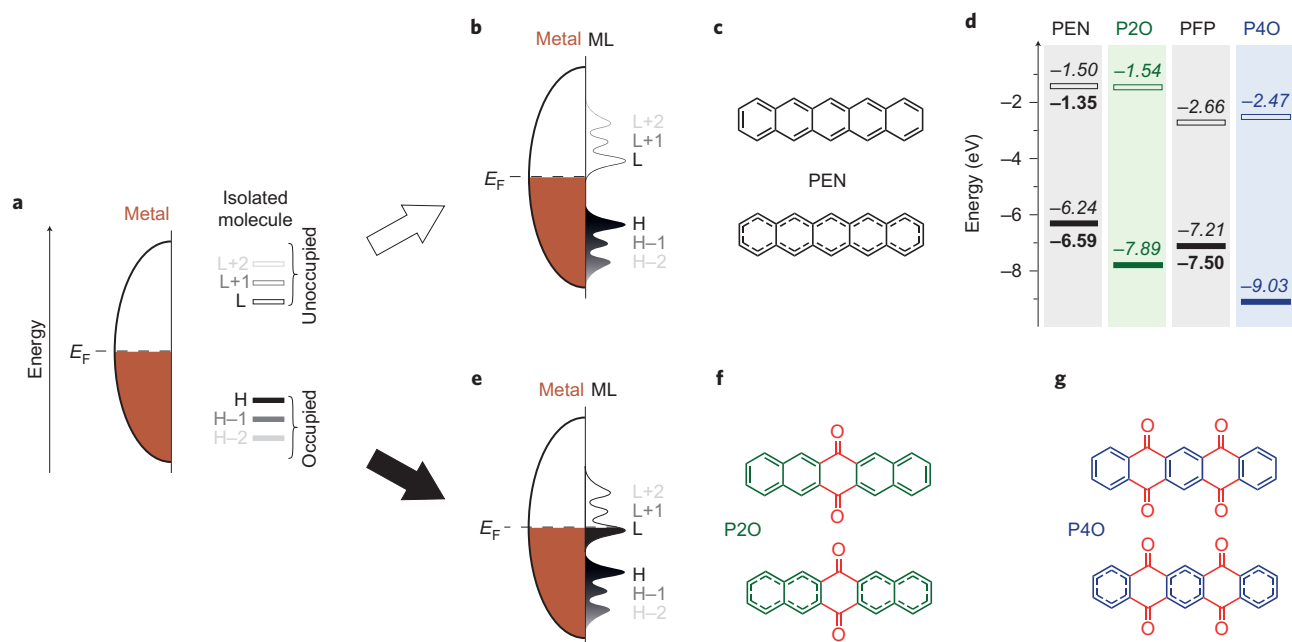


Figure 1 | Schematic of relevant energy levels and molecular structures. **a**, DOS and E_F of a metal and the highest occupied (H) as well as lowest unoccupied (L) orbitals of a free molecule. The lower-lying occupied (H-1, H-2) and higher-lying unoccupied molecular orbitals (L+1, L+2) are drawn in successively lighter grey to signify their successively waning importance for the phenomena discussed here. **b**, Commonly observed energy-level alignment between metal and molecular monolayer (ML). **c**, Chemical structure of PEN, with the π -electron delocalization highlighted by aromatic bonds in the lower panel. **d**, DFT calculated (italic) and experimental (bold)^{12,13} gas-phase ionization energies (filled bars) and electron affinities (open bars) of PEN, P2O, PFP and P4O. **e**, Energy-level alignment for the case of a partially filled LUMO and, thereby, a metallic molecular monolayer on a metal. **f, g**, Chemical structures of P2O (green, **f**) and P4O (blue, **g**) that indicate π -electron delocalization within the two conjugated naphthalene and three aromatic subunits, respectively, by aromatic bonds in the lower panels. The (keto) groups that disrupt full π -conjugation are highlighted in red.

via two keto groups, which break π -conjugation along the backbone, and P4O as three phenylene rings linked by two keto groups each. This results in substantially increased electronic gaps, whereas the calculated LUMOs of P2O and P4O are very close in energy to those of PEN and PFP, respectively (Fig. 1d). From the energy levels alone, we could, therefore, expect P2O and P4O to equally remain semiconducting on the (111) surfaces of the three coinage metals gold, silver and copper (with E_F systematically moving up in energy towards the molecular LUMOs in that order).

Results

Prior to discussing the electronic structure of these metal–molecule interfaces, it is important to know the actual geometric structure of the organic adsorbates. To resolve their atomic-scale lateral ordering, we performed low-temperature scanning tunnelling microscopy on molecular (sub)monolayers to deduce detailed structural models (Supplementary Section A), which served as an input for dispersion-corrected hybrid density functional theory (DFT) calculations. Furthermore, as electronic metal–molecule interaction hinges critically on their spatial separation, the vertical adsorption distances were determined by the normal-incidence X-ray standing waves (NIXSW) technique (Supplementary Fig. S3), which also provides access to the (potentially different) adsorption heights of distinct atomic species, and thus reveals intramolecular distortions, if present.

On Au(111) both PEN derivatives are at virtually identical adsorption heights of 3.2–3.3 Å, indicative of comparatively weak interaction, that is, physisorption (Fig. 2a). For P2O, the same is true on the Ag(111) surface with a lower work function. In marked contrast, for P4O, which exhibits a substantially lower LUMO (Fig. 1d), the average carbon adsorption distance (~ 2.7 Å) is much shorter than that on gold and the oxygen atoms bend downwards (by ~ 0.3 Å). These observations suggest a much stronger interaction of P4O with silver (compared to P2O with silver and

both molecules with gold) mediated by the oxygen atoms. Finally, on the even less noble copper, P2O, which exhibits the higher LUMO energy of the two molecules (Fig. 1d), also adsorbs with an average carbon height that is substantially smaller (~ 2.7 Å) than that on both Ag(111) and Au(111), and with the oxygens bent (by ~ 0.3 Å) towards the surface. P4O on Cu(111) is bent similarly as on Ag(111) with a further reduction of the overall adsorption height by ~ 0.4 Å.

To assess the consequences of these quite dramatic adsorption-induced molecular distortions on the chemical structure of the organic adsorbates, we performed X-ray photoelectron spectroscopy (XPS). The signal from the monolayers is contrasted to that of the respective thicker films to identify reliably the species that interact directly with the metal. For both molecules on Au(111), which are physisorbed only, we observe a single peak in the O1s region (Fig. 2b). The situation does not change for P2O on the lower work-function Ag(111), where this molecule with the higher LUMO of the two (Fig. 1d) is still bound only weakly. For P4O, however, which exhibits the lower LUMO and adsorbs at a much shorter vertical distance on Ag(111) in a distorted geometry (Fig. 2a), the monolayer O1s peak is shifted by almost 2 eV towards lower binding energies, which clearly marks the downwards-bent oxygens as different chemical species. On the even less noble Cu(111), where both P2O and P4O adsorb at a reduced vertical distance in a bent geometry, the monolayer O1s core levels of both molecules appear at a significantly lower binding energy.

The C1s core levels (Fig. 2c) exhibit concurring shifts: the same two peaks are observed in the mono- and multilayer XPS spectra of both P2O and P4O on Au(111), which, from their intensity ratio, are assigned readily to the aromatic (lower binding energy) and keto (higher binding energy) carbons, respectively. Again, the situation does not change for P2O physisorbed on Ag(111), whereas dramatic changes are seen for the distorted P4O. In particular, the

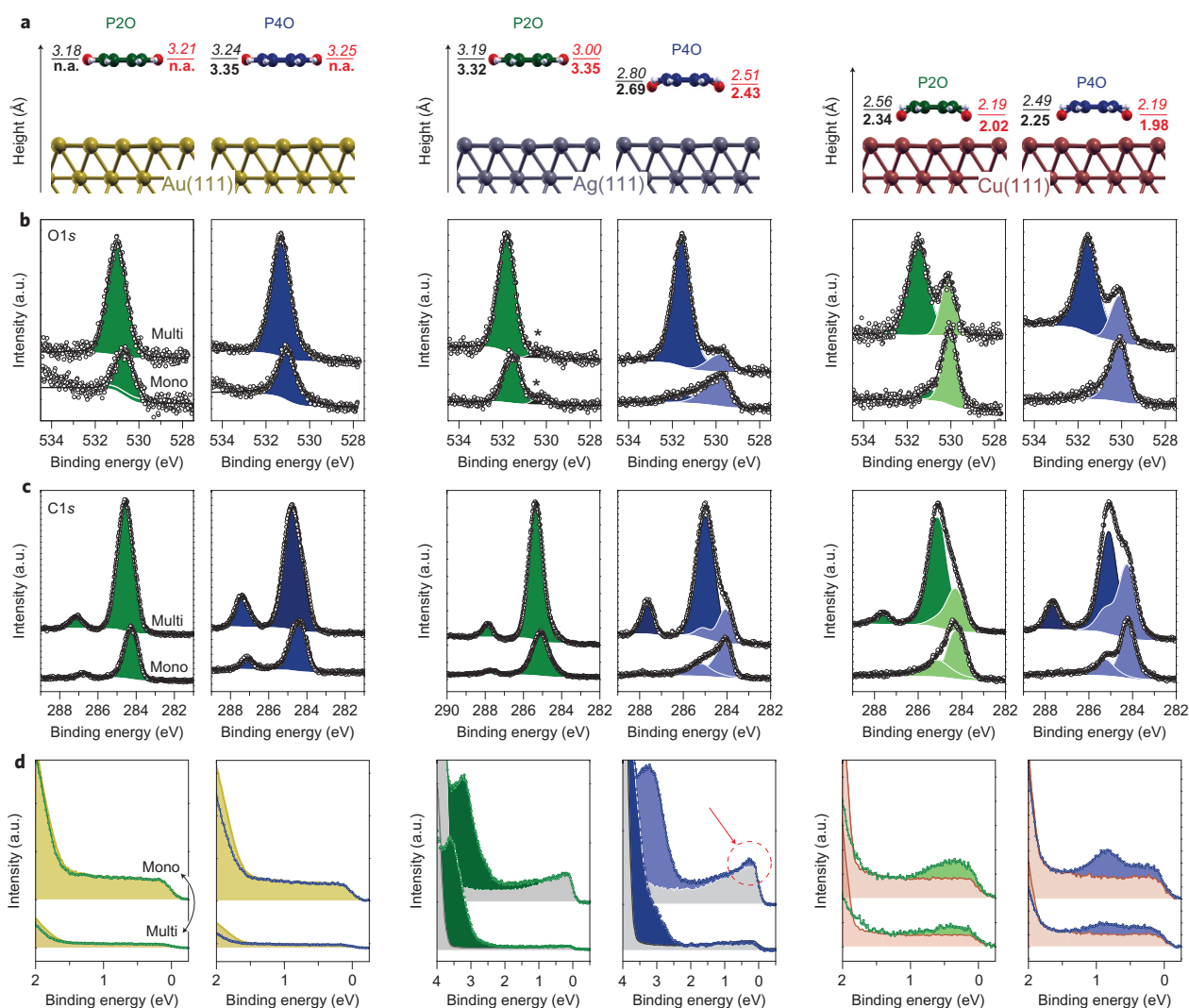


Figure 2 | Experimental results on structure, chemical nature and electronic structure. **a**, Vertical adsorption heights of P2O and P4O on the (111) surfaces of Au, Ag and Cu. Bold numbers refer to experimental (NIXSW) and italic numbers to theoretical results, black numbers to carbon and red numbers to oxygen. For better visibility, the molecular distortions are not drawn to scale. **b**, XPS spectra in the oxygen 1s core-level region for nominally 3 Å thick molecular monolayers (bottom traces) and nominally 30 Å thick multilayers (top traces). Lighter colours highlight new or changed features that correlate with shorter vertical adsorption distances and intramolecular distortions; we attribute the faint peak (*) at ~530 eV for P2O on Ag to residual oxygen contamination of the surface. **c**, Corresponding XPS spectra in the carbon 1s core-level region. **d**, Corresponding UPS spectra with the clean-substrate reference shown in gold, grey and light red for Au, Ag and Cu, respectively. The origin of the energy scale is set to E_F . For better visibility, the order of monolayer (top) and multilayer (bottom) traces is reversed compared with that in **b** and **c**. That monolayer features in XPS and the Fermi edge of the metal substrates in UPS are still visible at nominal multilayer coverage suggests a pronounced island growth of both molecules. In both XPS and UPS, minor shifts towards higher binding energies in multilayer compared to monolayer spectra are attributed to reduced photo hole screening by the metal. a.u. = arbitrary units, n.a. = not available.

peak associated with the keto carbons (at ~288 eV) vanishes, only to contribute to a double-peak structure in the aromatic region around 285 eV. Apparently, the two (formerly very different) carbon species are now in a much more similar chemical environment compared to that in the multilayer and purely physisorbed monolayer. Together with the changes in the corresponding O1s spectrum, this points towards an appreciable change in the chemical nature not only of the keto groups but, in fact, of the entire molecule. The XPS results on Cu(111) are consistent in that now the monolayer C1s spectrum of P2O is also changed, in the same way as that of P4O.

To correlate the observed peculiarities in adsorption geometry and chemical nature with the respective valence electronic structure, we performed ultraviolet photoelectron spectroscopy (UPS). On gold, no new photoemission features that could be related to the physisorbed molecules arose in the energy range down to 2 eV

below E_F . Given their high ionization energies (Fig. 1d), their HOMOs probably lie at an even higher binding energies, where they are masked by the strong gold *d*-band photoemission, the onset of which can be seen at the left edge of the respective plots in Fig. 2d. In the case of silver, with a lower work function, the *d*-band onset is at a significantly higher binding energy (~4 eV), which reveals that the photoemission feature associated with the HOMO of P2O indeed lies at ~3 eV (ref. 9). Importantly, additional photoemission intensity at E_F , attributed to occupied LUMO-derived states^{15–26}, is detected for monolayer P4O on Ag(111), where this molecule, with its higher electron affinity, adsorbs in a distorted geometry, at a reduced vertical bonding distance and with pronounced changes to its chemical nature. Finally, on the even less noble Cu(111), a partially filled broad LUMO-derived peak can be seen clearly for P2O also, and for P4O the Fermi level lies even higher in the broadened and formerly unoccupied DOS.

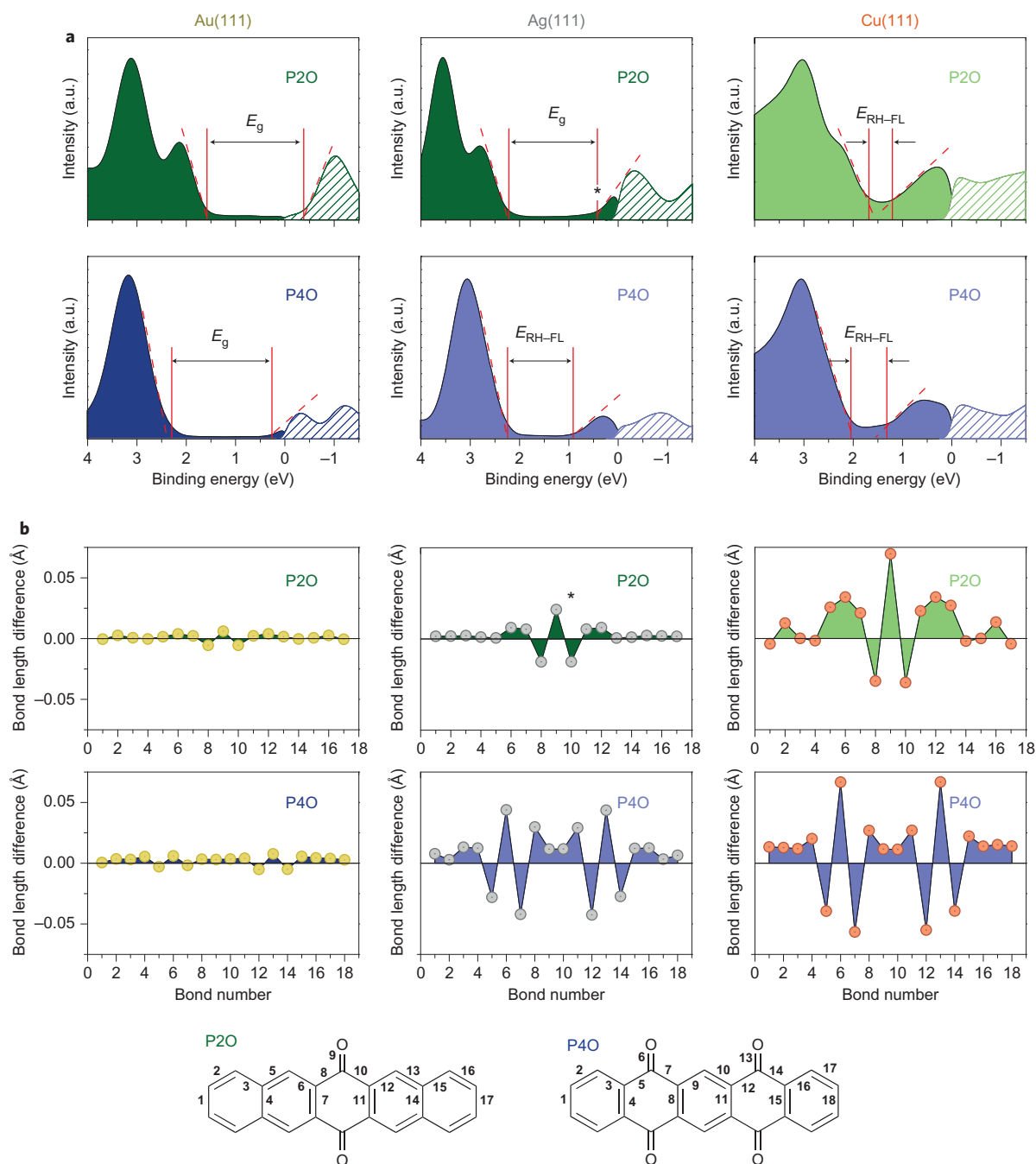


Figure 3 | Theoretical results on electronic structure and intramolecular distortions. **a**, DFT-calculated DOS projected onto the molecular adlayers, filled for occupied and hashed for unoccupied; the origin of the energy scale is set to E_F . Dashed red lines highlight the construction to find the HOMO and LUMO onsets and solid lines demarcate the fundamental gap (E_g), which is seen to be reduced (to E_{RH-FL}) on LUMO filling. The asterisk marks LUMO states of P2O on Ag(111) that spuriously tail down to below E_F because of the underestimation of the molecular gap even with the employed hybrid exchange-correlation functional. **b**, Adsorption-induced changes in intramolecular bond lengths numbered according to the schemes shown for P2O and P4O; as a consequence of spurious LUMO filling in the calculations, minor bond-length changes (*) are seen also for P2O on Ag(111), where none are expected given the absence of molecular DOS at E_F in the experimental UPS spectra (Fig. 2d).

To understand why LUMO filling occurs in these two molecules (and certain others) on coinage-metal (111) surfaces, even though no such phenomenon is observed for PEN, PFP and many more, despite comparable orbital energies and equally close adsorption distances¹¹, the DFT-calculated DOS projected onto the respective molecules adsorbed on each metal surface was analysed (Fig. 3a; for results on PEN and PFP, see Toyoda *et al.*^{28,29}). In the cases where experiment suggests strong metal–molecule interaction, that is, for P4O on Ag(111) and for both molecules on Cu(111),

the energy gap E_{RH-FL} between the relaxed HOMO (RH) and the now (partially) filled former LUMO (FL) is reduced drastically compared to the HOMO–LUMO gap E_g in the weakly interacting systems, similar to other reports of (partial) LUMO filling^{17–19,30,31}. Moreover, the concurrent changes in the chemical nature of the keto groups (apparent from the bent geometries and substantial changes in their XPS signature) can be specified further by analysing the adsorption-induced changes of the intramolecular bond lengths (Fig. 3b). Again reminiscent of reports on similar cases^{15–17}, a

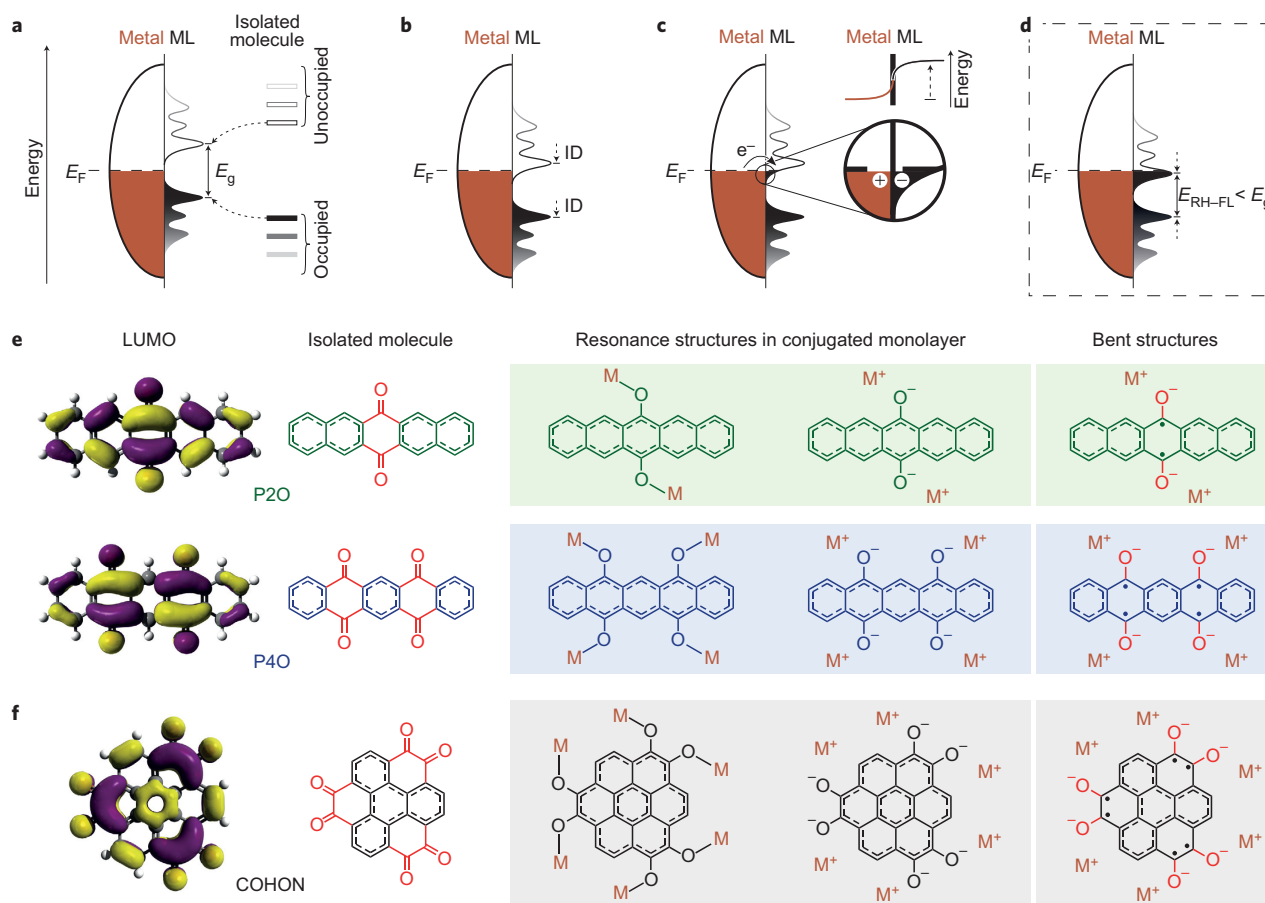


Figure 4 | Evolution of metal-molecule interfacial electronic structure and mechanism of surface-induced aromatic stabilization. **a**, Broadening of discrete molecular energy levels on approaching the metal (with Fermi level E_F) and reduction of the free-molecule gap to E_g . **b**, Rigid downwards shift of molecular states by the interface dipole (ID) with respect to E_F . **c**, Schematic of the mechanism of (quasi) Fermi-level pinning on charge transfer into LUMO states tailing down below E_F . **d**, Further reduction of E_g to E_{RH-FL} and lowering of the LUMO through the mechanism of surface-induced aromatic stabilization. **e**, From left to right: DFT-calculated LUMOs, chemical structures of the isolated molecules, fully π -conjugated resonance structures that gain in importance on the metal surface on LUMO filling and bent resonance structures on the surface. **f**, Same as **e** for a proposed compound in which surface-induced aromatic stabilization is predicted to occur. Chemical (keto) groups that interrupt full π -conjugation are highlighted in red.

pronounced lengthening of the C=O double bonds towards C–O single bonds is observed, accompanied by a shortening of the adjacent C–C single bonds (which link the keto groups to the naphthalene (P2O) or phenylene (P4O) segments) towards aromatic bonds.

Discussion

Combining all the structural, chemical and electronic information now permits us to derive a conclusive mechanism for the occurrence of partially occupied frontier orbitals in P2O and P4O monolayers on metals. We start with a summary of what is known on the formation of the metal–molecule interfacial electronic structure in general and why E_F should not readily cross into a molecular orbital in particular^{2–4,17}:

As a molecule approaches the surface and is attracted by weak dispersive interactions, both its ionization and affinity levels are stabilized energetically because the associated excess charges on the molecule (positive and negative, respectively) are attracted by their mirror images in the metal (Fig. 4a)^{3,17,30}. Consequently, the HOMO moves up in energy with respect to the isolated molecule, the LUMO moves down and, owing to hybridization with the metal states, the discrete molecular energy levels are broadened. Furthermore, the approaching molecule compresses the tail of the electron cloud, which is ‘leaking out’ into the vacuum above atomically clean metal surfaces, back into the metal, and thereby reduces its intrinsic surface dipole^{3,4,32}. As a consequence, the effective work

function that the molecule experiences is substantially lowered, which results in a rigid downwards shift by the interface dipole of all molecular states with respect to the metal Fermi level (Fig. 4b)^{2–4}. If, at this point, E_F comes to lie within the LUMO-derived molecular DOS, electrons are transferred from the metal into the LUMO tail, which results in a build-up of negative charge on the molecule compensated by a positively charged region in the metal surface (Fig. 4c). This dipolar charge distribution leads to a potential step across the metal–molecule interface that rigidly shifts all molecular states, the LUMO in particular, back up in energy, and thus acts to keep it above E_F . It is this mechanism of Fermi-level pinning that impedes the LUMO edge in crossing E_F in general^{3,4}, and for PEN and PFP monolayers on coinage-metal (111) surfaces in particular.

Any explanation as to why substantial LUMO filling still occurs in some molecules should thus provide a mechanism to overcome Fermi-level pinning, that is, to (over)compensate the upwards shift of the LUMO that sets in as soon as charge starts being transferred from metal to molecule (Fig. 4d). Our theoretical results (Fig. 3) together with the XPS data (Fig. 2b,c) clearly outline a simple and chemically intuitive mechanism as to why the LUMO is lowered drastically in energy and for which molecules (Fig. 4e). Starting with P2O, the calculated LUMO of the isolated molecule exhibits a node on the keto C=O double bonds. Initial charging of LUMO-derived states tailing below E_F on the metal with the

lowest effective work function, Cu(111), thus weakens and lengthens this bond towards a C–O single bond (Fig. 3b), which leads to a rehybridization of the oxygen (Fig. 2b). This, in turn, favours the formation of a covalent bond with the underlying metal surface. Furthermore, the LUMO exhibits an antinode on the C–C single bonds that connects the keto groups to the naphthalene subunits. Therefore, on the initial filling of the LUMO tail, these bonds are strengthened and shortened towards the aromatic regime (Fig. 3b). Although similar thoughts were expressed for other compounds^{15–17,25,27}, it was not recognized until now that, subsequently, the p_z -orbitals of (in our case) the keto carbons become successively incorporated into the conjugated π -system of the molecular backbone (Fig. 2c). Most importantly, the resonant structure that consequently gains in importance on adsorption-induced LUMO filling exhibits, like PEN, a fully π -conjugated backbone (Fig. 4e, centre left). In fact, the two formerly only weakly coupled naphthalene units are now fused into a single π -electron system (that of 6,13-pentacenediol), delocalized over the entire molecule. This increase of the effective conjugation length reduces the molecular gap ($E_g \rightarrow E_{RH-FL}$), which brings, in particular, the LUMO down in energy and thereby induces even more charge to flow onto the molecule until E_F finally lies well within the formerly unoccupied molecular DOS; an upper limit of -0.8 eV is estimated for this downwards shift of the P2O LUMO (Supplementary Section C.3).

To denote the charging of the molecule on the surface, it appears adequate to also attribute weight to the ionic ($-O^- \cdots M^+$) resonance structure (Fig. 4e, centre), which chemically rationalizes the bent molecular conformation as well. This is in analogy to benzophenone, in which, on reduction by alkali metals, the radical character of the resulting diphenylketyl is localized mainly on the ketyl carbon. Likewise, the (former) keto carbons in P2O can be seen as exhibiting, in part, a radical character on the Cu(111) surface (Fig. 4e, right) and so tend towards sp^3 hybridization; out-of-plane bending of the $C^{\bullet}-O^-$ bond is the obvious consequence. It is easy to see that the mechanism of surface-induced aromatic stabilization just described cannot occur in PEN or PFP, but that it does apply to P4O (Fig. 4e). Starting out with a lower initial LUMO than that of P2O, the mechanism is operative already on the more noble Ag(111) surface, on which P4O is, effectively, converted into 5,7,12,14-pentacenetetrol.

Although P2O and P4O are singularly well-suited to demonstrate the mechanism that underlies the phenomenon of surface-induced aromatic stabilization, its applicability is by no means limited to this particular pair of molecules. In fact, several other systems that exhibit (partial) LUMO filling on metal surfaces^{15–22} are likely to follow the same scheme, as discussed in Supplementary Section C. To provide, in addition, a testable prediction that emerges from our model, we propose in Fig. 4f a candidate molecule, 1,2,5,6,9,10-coronenehexone (COHON), for concurrently observing the phenomena associated with surface-induced aromatic stabilization; that is, a bent adsorption geometry, characteristic (differential) mono-to-multilayer shifts for the oxygen and carbon core levels, and a (partially) occupied LUMO-derived DOS at E_p , not on gold³³, but at least on Cu(111) and possibly already on Ag(111) surfaces. Moreover, the mechanism proposed here is not restricted to oxygens (keto or carboxylic^{15–21}) establishing the link to the metal. Although limitations to our model are addressed in Supplementary Section C.5, it seems to apply equally to a number of cases in which the bond to the metal is formed via cyano groups, which are common motifs in strong molecular acceptors^{7,23–27} (Supplementary Section C.2). Note that, for some systems, the (broadened) LUMO appears not partially but completely filled, lying entirely below the Fermi level with no molecular DOS visible at E_F by UPS^{19–26}; albeit considerably charged, it is thus more appropriate to regard such species as (again) semiconducting. Although the main focus of the present article is on (partial) LUMO

filling in electron-acceptor molecules, it is remarkable to see that the very same mechanism of surface-induced aromatic stabilization also seems to hold for certain electron donors, in which (partial) HOMO emptying is observed on metals with a high effective work function such as gold (Supplementary Section C.4)^{34–36}, as well as for specific self-assembled monolayers³⁷.

Conclusions

To summarize, we started out with the question as to why certain π -conjugated molecules more readily allow the Fermi level of a metal to cross into their frontier orbitals, their LUMO in particular, than do others. We found that resonance structures have to exist, which, when stabilized on the surface through initial metal-to-molecule charge transfer and concomitant rehybridization of suitable side groups, exhibit a significantly extended π -electron system that is coupled strongly to the metal states. The ensuing reduction of the molecular electronic gap (the lowering of the LUMO in particular) then aids in overcoming the competing phenomenon of Fermi-level pinning, and thus leads to substantially charged molecular monolayers, which, provided E_F comes to lie within a (broadened) frontier molecular orbital, behave metallically for all practical purposes. This mechanism of surface-induced aromatic stabilization appears to be operative in many cases in which the filling of LUMO-derived or emptying of HOMO-derived electronic states is reported on metal surfaces. Our findings suggest building up a library of precursors (with overall affinity and ionization levels well within the environmental stability window) that consist of π -conjugated segments interrupted by electron-accepting (for example, keto) or -donating groups. Charge-transfer interaction with and/or bonding to a metal surface or nanostructure then allows these precursors to attain their full degree of π -conjugation (and therefore an exceedingly low gap) by fusing smaller subunits into a single and considerably larger π -system that is coupled strongly to the metal states around the Fermi level. Such species can be expected to open up new possibilities for chemical surface engineering in applications where metallic, and yet molecular, electrodes are desirable, such as for biocompatible coatings or for molecular and organic electronics. Especially regarding the latter, we see the potential for simultaneously eliminating unwanted energy barriers for charge-carrier injection^{3–5} and providing a template for stimulating the desired growth mode of a subsequently deposited organic semiconductor.

Methods

P2O and P4O were purchased from Sigma Aldrich, purified via resublimation prior to use and deposited from resistively heated quartz crucibles onto atomically clean metal single crystals (repeated Ar⁺-ion sputtering and annealing cycles up to 550 °C). The nominal film thicknesses were monitored with a quartz microbalance. Sample preparation and all measurements proceeded at room temperature.

NIXSW experiments were done in back-reflection geometry at beamline ID32 of the European Synchrotron Radiation Facility (ESRF, Grenoble, France)³⁸. The evaporation rate was ~ 0.25 Å min⁻¹ and the nominal coverage was around 1 Å. The measurements on Ag(111) and Cu(111) were done in the 'XSW chamber' (base pressure 3×10^{-10} mbar) with the electron analyser mounted at an angle of 45° relative to the incoming X-ray beam, and the measurements on Au(111) were made in the 'HAXPES chamber' (base pressure 2×10^{-10} mbar) with a photoelectron emission angle close to 90°. The NIXSW data were analysed using the software package DARE (developed at the ESRF).

The standing wave formed by the incident and Bragg-reflected X-ray beam excites photoelectrons in the adsorbed molecules. If the energy of the X-rays is scanned through the Bragg condition, the intensity variation of the emitted electrons can be used to determine the average distance between a distinct atomic species and the substrate. The NIXSW photoelectron yield (Y_p) is given by equation (1)^{39,40}:

$$Y_p = 1 + R + 2\sqrt{R}f_H \cos(\nu - 2\pi P_H) \quad (1)$$

with R the reflectivity and ν the phase factor. It allows determination of both the coherent fraction (f_H), which is a measure for the degree of order within the

adsorbate layer, and the coherent position (P_H), from which the element-specific bonding distance (d_H) can be deduced. The non-dipole contributions to the XPS spectra collected at an emission angle of 45° were taken into account⁴¹. As the NIXSW technique averages over macroscopic areas of the sample, it is very sensitive to static and dynamic disorder in the adsorbate layer. Therefore, the coherent fraction often deviates significantly from unity. The coherent positions, however, are rather robust⁴², which results in a typical precision of $\Delta d_H = \pm 0.05 \text{ \AA}$, except for the oxygens of P2O, for which the low intensity of the O1s signal reduces the precision to $\Delta d_H = \pm 0.1 \text{ \AA}$. The oxygen bonding distance on Au(111) cannot be determined experimentally because the O1s signal overlaps with the gold Auger emission in the relevant photon-energy range⁴³.

Photoemission experiments were performed at the end station SurfCat (beamline PM4) of the synchrotron light source BESSY II (Berlin, Germany) using photon energies of 620 eV and 35 eV for XPS and UPS, respectively. XPS (UPS) spectra were collected at a 0° (45°) take-off angle with a hemispherical electron-energy analyser, Scienta SES 100. Evaporation rates were 2 \AA min^{-1} . The pressure during evaporation did not exceed 5×10^{-8} mbar and samples were transferred to the analysis chamber (base pressure 2×10^{-10} mbar) without breaking the ultrahigh vacuum conditions.

Based on the experimentally determined surface unit cells (Supplementary Section A), periodic DFT calculations on the metal–molecule interfaces were performed with the Vienna *ab initio* Simulation Package (VASP)⁴⁴ in the repeated-slab approach with four atomic layers representing the metal surfaces. To avoid spurious interaction between consecutive images of the slab along the surface normal, a vacuum region of $\sim 20 \text{ \AA}$ was introduced with an artificial dipole layer in the middle to compensate for the net dipole moment of the slab. To describe the valence–core interactions, the projector augmented-wave method⁴⁵ was applied and the valence Kohn–Sham pseudo-wavefunctions were expanded in a plane-wave basis with a cutoff of 30 Ryd. A lateral Monkhorst–Pack k -point grid equivalent to 15×15 in the primitive (111) surface unit cell was used together with a Methfessel–Paxton occupation scheme (smearing 0.2 eV). For geometry optimizations, all atoms of the adsorbed molecules and the top two layers of metal were relaxed until the residual forces were $< 10^{-2} \text{ eV \AA}^{-1}$ using the gradient-corrected exchange–correlation functional of Perdew, Burke and Ernzerhof⁴⁶, including Grimme-type van der Waals corrections with accordingly⁴⁷ determined parameters ($C_6 = 43.63 \text{ J-nm}^6\text{-mol}^{-1}$ and $R_0 = 1.732 \text{ \AA}$) for gold. Although newer developments to describe dispersive metal–molecule interactions are fundamentally more appealing⁴⁸, Grimme-type corrections have been shown to yield good results for both PEN and PFP on coinage-metal (111) surfaces^{28,29}. Finally, the electronic structure of the relaxed geometries was calculated using the range-separated hybrid exchange–correlation functional of Heyd, Scuseria and Ernzerhof (HSE06)⁴⁹, which, to some extent, improves the well-known underestimation of band gaps produced by (semi)local functionals⁵⁰. For better comparison with the experiments, the resulting projected DOS was broadened with a Gaussian line shape (full-width at half-maximum of 0.5 eV) and multiplied with a respective Fermi function ($k_B T = 50 \text{ meV}$ to mimic finite experimental resolution) for occupied and unoccupied states.

Calculations on isolated molecules in the gas phase were performed using the HSE06 functional, both for geometry optimization and electronic-structure determination, in conjunction with a triple- ζ valence contracted-Gaussian basis set, including one set each of additional polarization and diffuse functions on all atoms (6-311++G**). Vertical ionization energies and electron affinities were computed in the delta self-consistent field approach, that is, as total energy differences between neutral molecules and respectively charged ions.

Received 13 September 2012; accepted 10 January 2013;
published online 17 February 2013

References

- Netzer, F. P. & Ramsey, M. G. Structure and orientation of organic molecules on metal surfaces. *Crit. Rev. Solid State* **17**, 397–475 (1992).
- Ishii, H., Sugiyama, K., Ito, E. & Seki, K. Energy level alignment and interfacial electronic structures at organic/metal and organic/organic interfaces. *Adv. Mater.* **11**, 605–625 (1999).
- Braun, S., Salaneck, W. R. & Fahlman, M. Energy-level alignment at organic/metal and organic/organic interfaces. *Adv. Mater.* **21**, 1450–1472 (2009).
- Hwang, J., Wan, A. & Kahn, A. Energetics of metal–organic interfaces: new experiments and assessment of the field. *Mater. Sci. Eng. Rep.* **64**, 1–31 (2009).
- Koch, N. Organic electronic devices and their functional interfaces. *Chem. Phys. Chem.* **8**, 1438–1455 (2007).
- Hipps, K. W. Molecular electronics – it's all about contacts. *Science* **294**, 536–537 (2001).
- Glowatzki, H. *et al.* 'Soft' metallic contact to isolated C_{60} molecules. *Nano Lett.* **8**, 3825–3829 (2008).
- Jaegel, B., Sambur, J. B. & Parkinson, B. A. The influence of metal work function on the barrier heights of metal/pentacene junctions. *J. Appl. Phys.* **103**, 063719 (2008).

- Koch, N. *et al.* Molecular orientation dependent energy levels at interfaces with pentacene and pentacenequinone. *Org. Electron.* **7**, 537–545 (2006).
- Koch, N., Vollmer, A., Duhm, S., Sakamoto, Y. & Suzuki, T. The effect of fluorination on pentacene/gold interface energetics and charge reorganization energy. *Adv. Mater.* **19**, 112–116 (2007).
- Koch, N. *et al.* Adsorption-induced intramolecular dipole: correlating molecular conformation and interface electronic structure. *J. Am. Chem. Soc.* **130**, 7300–7304 (2008).
- Crocker, L., Wang, T. B. & Kebarle, P. Electron-affinities of some polycyclic aromatic-hydrocarbons, obtained from electron-transfer equilibria. *J. Am. Chem. Soc.* **115**, 7818–7822 (1993).
- Delgado, M. C. R. *et al.* Impact of perfluorination on the charge-transport parameters of oligoacene crystals. *J. Am. Chem. Soc.* **131**, 1502–1512 (2009).
- Duhm, S. *et al.* Influence of intramolecular polar bonds on interface energetics in perfluoro-pentacene on Ag(111). *Phys. Rev. B* **81**, 045418 (2010).
- Hauschild, A. *et al.* Molecular distortions and chemical bonding of a large π -conjugated molecule on a metal surface. *Phys. Rev. Lett.* **94**, 036106 (2005).
- Rohlfing, M., Temirov, R. & Tautz, F. S. Adsorption structure and scanning tunneling data of a prototype organic–inorganic interface: PTCDA on Ag(111). *Phys. Rev. B* **76**, 115421 (2007).
- Tautz, F. S. Structure and bonding of large aromatic molecules on noble metal surfaces: the example of PTCDA. *Prog. Surf. Sci.* **82**, 479–520 (2007).
- Bendounan, A. *et al.* Electronic structure of 1 ML NTCDA/Ag(111) studied by photoemission spectroscopy. *Surf. Sci.* **601**, 4013–4017 (2007).
- Kilian, L. *et al.* Role of intermolecular interactions on the electronic and geometric structure of a large π -conjugated molecule adsorbed on a metal surface. *Phys. Rev. Lett.* **100**, 136103 (2008).
- Ziroff, J. *et al.* Low-energy scale excitations in the spectral function of organic monolayer systems. *Phys. Rev. B* **85**, 161404 (2012).
- Duhm, S. *et al.* PTCDA on Au(111), Ag(111) and Cu(111): correlation of interface charge transfer to bonding distance. *Org. Electron.* **9**, 111–118 (2008).
- Duhm, S. *et al.* Weak charge transfer between an acceptor molecule and metal surfaces enabling organic/metal energy level tuning. *J. Phys. Chem. B* **110**, 21069–21072 (2006).
- Koch, N. *et al.* Tuning the hole injection barrier height at organic/metal interfaces with (sub)monolayers of electron acceptor molecules. *Appl. Phys. Lett.* **87**, 101905 (2005).
- Koch, N., Duhm, S., Rabe, J. P., Vollmer, A. & Johnson, R. L. Optimized hole injection with strong electron acceptors at organic–metal interfaces. *Phys. Rev. Lett.* **95**, 237601 (2005).
- Romaner, L. *et al.* Impact of bidirectional charge transfer and molecular distortions on the electronic structure of a metal–organic interface. *Phys. Rev. Lett.* **99**, 256801 (2007).
- Rangger, G. M. *et al.* F4TCNQ on Cu, Ag, and Au as prototypical example for a strong organic acceptor on coinage metals. *Phys. Rev. B* **79**, 165306 (2009).
- Tseng, T. C. *et al.* Charge-transfer-induced structural rearrangements at both sides of organic/metal interfaces. *Nature Chem.* **2**, 374–379 (2010).
- Toyoda, K., Hamada, I., Lee, K., Yanagisawa, S. & Morikawa, Y. Density functional theoretical study of pentacene/noble metal interfaces with van der Waals corrections: vacuum level shifts and electronic structures. *J. Chem. Phys.* **132**, 134703 (2010).
- Toyoda, K., Hamada, I., Lee, K., Yanagisawa, S. & Morikawa, Y. Density functional theoretical study of perfluoropentacene/noble metal interfaces with van der Waals corrections: adsorption states and vacuum level shifts. *J. Phys. Chem. C* **115**, 5767–5772 (2011).
- Amy, F., Chan, C. & Kahn, A. Polarization at the gold/pentacene interface. *Org. Electron.* **6**, 85–91 (2005).
- Tsipser, E. V., Soos, Z. G., Gao, W. & Kahn, A. Electronic polarization at surfaces and thin films of organic molecular crystals: PTCDA. *Chem. Phys. Lett.* **360**, 47–52 (2002).
- Witte, G., Lukas, S., Bagus, P. S. & Wöll, C. Vacuum level alignment at organic/metal junctions: 'cushion' effect and the interface dipole. *Appl. Phys. Lett.* **87**, 263502 (2005).
- Medjanik, K. *et al.* Electronic structure of large disc-type donors and acceptors. *Phys. Chem. Chem. Phys.* **12**, 7184–7193 (2010).
- Bröker, B. *et al.* Gold work function reduction by 2.2 eV with an air-stable molecular donor layer. *Appl. Phys. Lett.* **93**, 243303 (2008).
- Hofmann, O. T., Rangger, G. M. & Zojer, E. Reducing the metal work function beyond Pauli pushback: a computational investigation of tetrathiafulvalene and viologen on coinage metal surfaces. *J. Phys. Chem. C* **112**, 20357–20365 (2008).
- Fernandez-Torrente, I. *et al.* Long-range repulsive interaction between molecules on a metal surface induced by charge transfer. *Phys. Rev. Lett.* **99**, 176103 (2007).
- Rissner, F. *et al.* Radical self-assembled monolayers on Au(111) formed by the adsorption of closed-shell molecules. *J. Mater. Chem.* **22**, 4269–4272 (2012).
- Zegenhagen, J. *et al.* X-ray standing waves and hard X-ray photoelectron spectroscopy at the insertion device beamline ID32. *J. Electron Spectrosc. Relat. Phenom.* **178**, 258–267 (2010).
- Woodruff, D. P. Surface structure determination using X-ray standing waves. *Rep. Prog. Phys.* **68**, 743–798 (2005).

40. Zegenhagen, J. Surface-structure determination with X-ray standing waves. *Surf. Sci. Rep.* **18**, 199–271 (1993).
41. Gerlach, A. *et al.* Adsorption-induced distortion of $F_{16}CuPc$ on Cu(111) and Ag(111): an X-ray standing wave study. *Phys. Rev. B* **71**, 205425 (2005).
42. Gerlach, A. *et al.* Orientational ordering of nonplanar phthalocyanines on Cu(111): strength and orientation of the electric dipole moment. *Phys. Rev. Lett.* **106**, 156102 (2011).
43. Henze, S. K. M., Bauer, O., Lee, T. L., Sokolowski, M. & Tautz, F. S. Vertical bonding distances of PTCDA on Au(111) and Ag(111): relation to the bonding type. *Surf. Sci.* **601**, 1566–1573 (2007).
44. Kresse, G. & Furthmüller, J. Efficiency of *ab-initio* total energy calculations for metals and semiconductors using a plane-wave basis set. *Comp. Mater. Sci.* **6**, 15–50 (1996).
45. Kresse, G. & Joubert, D. From ultrasoft pseudopotentials to the projector augmented-wave method. *Phys. Rev. B* **59**, 1758–1775 (1999).
46. Perdew, J. P., Burke, K. & Ernzerhof, M. Generalized gradient approximation made simple. *Phys. Rev. Lett.* **77**, 3865–3868 (1996).
47. Grimme, S. Semiempirical GGA-type density functional constructed with a long-range dispersion correction. *J. Comput. Chem.* **27**, 1787–1799 (2006).
48. Ruiz, V. G., Liu, W., Zojer, E., Scheffler, M. & Tkatchenko, A. Density-functional theory with screened van der Waals interactions for the modeling of hybrid inorganic–organic systems. *Phys. Rev. Lett.* **108**, 146103 (2012).
49. Heyd, J., Scuseria, G. E. & Ernzerhof, M. Hybrid functionals based on a screened Coulomb potential. *J. Chem. Phys.* **124**, 219906 (2006).
50. Biller, A., Tamblyn, I., Neaton, J. B. & Kronik, L. Electronic level alignment at a metal–molecule interface from a short-range hybrid functional. *J. Chem. Phys.* **135**, 164706 (2011).

Acknowledgements

The authors thank S. Hecht and Q. Xin for critically reading the manuscript, E. Zojer for fruitful discussions and O. T. Hofmann for providing the van der Waals parameters of gold. This work was supported by the Global Centres of Excellence Program of the Ministry of Education, Culture, Sports, Science and Technology (G03: Advanced School for Organic Electronics, Chiba University), and by the German Research Foundation through projects FR2726/1, SFB658, SFB951, SPP1355 and SCHR700/14-1. T.H. gratefully acknowledges an Alexander von Humboldt fellowship for foreign researchers.

Author contributions

G.H., S.D., I.S., C.B., S.W., A.W., R.S., J.F., B.B. and A.V. performed the XPS and UPS measurements and pre-processed the data. With A.G. leading the efforts, S.D., J.N., C.B., T.H. and B.D. performed NIXSW experiments and analysed the data. A.S., I.F.-T. and G.S. performed the scanning tunnelling microscopy measurements under the guidance of K.J.F. and J.I.P. J.P. provided the purified materials. I.S. analysed the XPS and UPS data and prepared the figures. With significant input from S.K. and N.U., G.H. and S.D. interpreted the overall results. G.H. performed the calculations, coordinated the work and wrote the paper. A.G., F.S. and N.K. conceived the project and all the authors commented critically on the manuscript.

Additional information

Supplementary information is available in the [online version](#) of the paper. Reprints and permission information is available online at <http://www.nature.com/reprints>. Correspondence and requests for materials should be addressed to G.H. and S.D.

Competing financial interests

The authors declare no competing financial interests.